

# Adaptive Self-Distillation for Minimizing Client Drift in Heterogeneous Federated Learning

M Yashwanth<sup>1</sup> Gaurav Kumar Nayak<sup>2</sup> Arya Singh<sup>1</sup> Yogesh Simmhan<sup>1</sup> Anirban Chakraborty<sup>1</sup>

## Abstract

Federated Learning (FL) is a machine learning paradigm that enables clients to jointly train a global model by aggregating the locally trained models without sharing any local training data. In practice, there can often be substantial heterogeneity (e.g., class imbalance) across the local data distributions observed by each of these clients. Under such non-iid data distributions across clients, FL suffers from the ‘client-drift’ problem where every client drifts to its own local optimum. This results in slower convergence and poor performance of the aggregated model. To address this limitation, we propose a novel regularization technique based on adaptive self-distillation (ASD) for training models on the client side. Our regularization scheme adaptively adjusts to the client’s training data based on the global model entropy and the client’s label distribution. The proposed regularization can be easily integrated atop existing, state-of-the-art FL algorithms, leading to a further boost in the performance of these off-the-shelf methods. We theoretically explain how ASD reduces client-drift and also explain its generalization ability. We demonstrate the efficacy of our approach through extensive experiments on multiple real-world benchmarks and show substantial gains in performance over state-of-the-art methods. The code is provided in the supplementary.

## 1. Introduction

Federated Learning (FL) is a machine learning method where the clients learn a shared model under the orchestration of the server without sharing the client’s data. Due to its privacy-preserving nature, it has many applications in smartphones (Hard et al., 2018; Ramaswamy et al., 2019), the Internet of Things (IoT), healthcare organizations (Rieke

<sup>1</sup>Indian Institute of Science, Bangalore, India <sup>2</sup>University of Central Florida, USA. Correspondence to: M Yashwanth <yashwanthm@iisc.ac.in>.

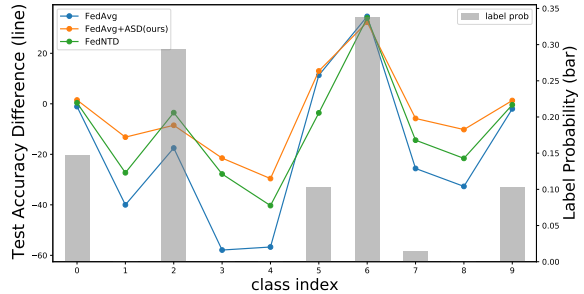


Figure 1. Impact of local learning on the test accuracy with CIFAR-10. The effect of local learning on test accuracy is assessed by plotting the accuracy difference before and after local training (line). Positive values indicate an improvement in model accuracy post-training. It is clear that in cases where the label distribution (bar) is sparse, models experience a decline in accuracy after local training. However, our proposed adaptive self-distillation method not only preserves knowledge on imbalanced classes but also effectively learns from classes with over-representation.

et al., 2020; Xu et al., 2021), etc. where training data is generated at edge devices or from privacy-sensitive domains. As originally introduced in (McMahan et al., 2017), FL involves model training across a distributed system consisting of one server and multiple clients. In traditional FL, each client securely holds its training data, due to privacy concerns and to avoid large communication overheads if transmitting it externally. At the same time, these clients aim to collaboratively train a generalized model that can leverage the entirety of the training data disjointly distributed across clients. Data generated at the edge/client devices are often highly heterogeneous, as a consequence of the data generation process. They can differ in terms of quantity imbalance (the number of samples with each client), label imbalance (empirical label distribution across the clients), and feature imbalance (features of the data across the clients are non-iid). When there exists a label or feature imbalance, the training objective for every client becomes different as the local minimum for every client will be different. In such settings, during the local training, the client’s model starts to drift towards its local minimum and farther away from the global objective. This is undesirable as the goal of the FL is

---

to converge to a global model that generalizes well across all the clients. This phenomenon, known as ‘client-drift’, is introduced and explored in earlier works (Karimireddy et al., 2020; Acar et al., 2021; Wang et al., 2021). Due to this, client models tend to forget the knowledge of the global model and overfit to their local data.

One popular way of mitigating this challenge of label imbalance across clients is via client-side regularization. Here, the local model trained by the client is explicitly regularized with the global model parameters to minimize client drift. Algorithms such as FedProx (Li et al., 2020), SCAF-FOLD (Karimireddy et al., 2020), and FedDyn (Acar et al., 2021) use regularization at the client-side in the parameter space. However, they ignore the representations of the global model, which can be useful and are explored in recent distillation-based works (He et al., 2022b; Lee et al., 2022). The primary motivation behind distillation and regularization for FL is to allow the global model to have better representations than the local models.

Recently (He et al., 2022b) introduced the class-wise adaptive weighting scheme FedCAD at the server side. Its major drawback is that it assumes the presence of related auxiliary data on the server in a reliable manner for computing the adaptive class-wise weights. Another work (Lee et al., 2022) proposes FedNTD which analyses the case of distilling only the incorrect class labels. The key issue with the existing distillation works is that they cannot explain how the generalization ability of the global model is improved.

To address these issues, motivated by client model regularization in mitigating client drift and to remove dependency on the server for computing client-side weights, we introduce an efficient strategy known as *Adaptive Self-Distillation (ASD)* for Federated Learning. Importantly, ASD does not require any auxiliary data. We use the KL divergence between the global and local models as the regularizer, and the per-sample weights for the regularizer are adaptively adjusted based on the global model entropy and the empirical label distribution of the client’s data. In Fig 1, we analyze the impact of client-drift by observing one round of local training on a particular client model with the CIFAR-10 dataset. We see that the performance of FedAvg on the labels that have sparse or no representation in its data is substantially deteriorates. However, after adding the ASD loss this impact is reduced. ASD performs the best in terms of local learning and preserving the global model knowledge on the sparse classes. *Later, we theoretically explain the client-drift reduction through our proposed ASD regularizer. In addition, we also provide justification that ASD leads to the generalized global model.* This novel design of our proposed method can be easily integrated over any existing FL methods to result in substantial performance gain, which makes it an attractive and compelling solution to the

federated learning problem. As a validation, we combine our proposed regularization scheme with algorithms such as FedAvg (McMahan et al., 2017), FedProx (Li et al., 2020), FedDyn (Acar et al., 2021) FedSpeed (Sun et al., 2023), FedNTD (Lee et al., 2022), FedSAM (Caldarola et al., 2022) and FedDisco (Ye et al., 2023). *To the best of our knowledge, this is the first work where the adaptive weights are used for the distillation loss in the FL framework without requiring auxiliary data and without the assistance of the server.*

The key contributions of this work are:

1. We introduce a novel regularization method ASD for Federated Learning that alleviates the client drift problem by adaptively weighting the regularization loss for each sample based on global model entropy and the label distribution of client data (§ 3.2).
2. We present the theoretical analysis of client-drift and show that our regularizer minimizes it (§ 3.3). We also show that ASD promotes better generalization by converging to a flat minimum (§ 3.4).
3. We demonstrate the efficiency of our method by extensive experiments on CIFAR-10, CIFAR-100, and Tiny-ImageNet (§ 4). We show the modularity of our ASD regularizer by combining it with state-of-the-art methods and improving their performance (§ 5).

## 2. Related Work

### 2.1. Federated Learning (FL)

In recent times, addressing non-iid problems in Federated Learning has become an active area of research, and the field is developing rapidly. For brevity, we discuss a few related works here. In FedAvg (McMahan et al., 2017), the two main challenges explored are reducing communication costs (Yadav & Yadav, 2016) and ensuring privacy by avoiding having to share the data. There are some studies based on gradient inversion (Geiping et al., 2020) raising privacy concerns owing to gradient sharing while others have proposed in defense of sharing the gradients (Kairouz et al., 2021; Huang et al., 2021). FedAvg is the generalization of local SGD (Stich, 2018) by increasing the number of local updates. It significantly reduces the communication costs in an iid setting, but does not give similar improvements for non-iid data. FedProx (Li et al., 2020) introduces a proximal term by penalizing the weights if they are far from the global initialized model. SCAFFOLD (Karimireddy et al., 2020) views this problem as one of objective inconsistency and introduces a gradient correction term that acts as a regularizer. Later, FedDyn (Acar et al., 2021) improves upon this by introducing the dynamic regularization term. (Zhang et al., 2020) attempts to solve this problem by enabling all device participation or none, as described by (Acar et al., 2021). Several papers perform an SGD-type analysis that involves the full device participation, and this breaks the

important constraint in FL setup of partial device participation. Some of these attempt to compress the models to reduce the communication cost (Mishchenko et al., 2019). A few works include regularization methods on the client side (Zhu et al., 2021), and one-shot methods where clients send the condensed data and the server trains on the condensed data (Zhou et al., 2020). In (Hsu et al., 2020), an adaptive weighting scheme is considered on task-specific loss to minimize the learning from samples whose representation is negligible. Flatness-based methods based on SAM called as FedSAM is introduced in (Qu et al., 2022; Caldarola et al., 2022).

## 2.2. Federated Learning using Knowledge Distillation

*Knowledge Distillation (KD)* introduced by (Hinton et al., 2015) is a technique to transfer the knowledge from a pre-trained teacher model to the student model by matching the predicted probabilities. Self-distillation was introduced in (Zhang et al., 2019) where the student distills from the same model to the sub-networks of the model. The teacher model’s predictions are updated every batch. In our method, distillation happens with the full network, and the teacher’s predictions are updated after every communication round. Adaptive distillation was used in (Tang et al., 2019). The server-side KD methods such as FedGen (Seo et al., 2022) use KD to train the generator at the server and the generator is broadcasted to the clients in the subsequent round. The clients use the generator to generate the data to provide the inductive bias. This method incurs extra communication of generator parameters along with the model and training of the generator in general is difficult. In FedDF (Lin et al., 2020) KD is used at the server that relies on the external data. The KD is performed on an ensemble of client models, especially client models acts as multiple teacher models and the knowledge is distilled into a single student model, which is a global model. In FedNTD (Lee et al., 2022) the non-true class logits are used for distillation. This method gives uniform weight to all the samples. In FedCAD (He et al., 2022b) and FedSSD (He et al., 2022a) the client-drift problem is posed as a forgetting problem, and a weighting scheme has been proposed. Importantly, the weights are assisted by the server with the assumption that the server has access to auxiliary data. One of its shortcomings is the availability of auxiliary data on the server, which may not hold. In (Zhang et al., 2022) logits were calibrated based on the label distribution. This is totally different from our approach as we are adjusting the weights of the distillation loss. Unlike all of these approaches, we propose a novel adaptive distillation strategy that aims to mitigate the challenge of client drift due to non-iid data without relying on the server and access to any form of auxiliary data to compute the adaptive weights.

## 3. Method

We first describe the federated optimization problem in general, then explain the proposed method of Adaptive Self-Distillation (ASD) in Section 3.2. We provide the theoretical and empirical analysis in the Sections 3.3 and 3.4, respectively.

### 3.1. Problem Setup

We assume that there is a single cloud server and  $m$  clients (edge devices). We further assume that client  $k$  has the Dataset  $\mathcal{D}_k$  with  $n_k$  training samples drawn iid from the data distribution  $\mathbb{P}_k(x, y)$ . The data distributions  $\{\mathbb{P}_k(x, y)\}_{k=1}^K$  across the clients are assumed to be non-iid. In this setup, we perform the following optimization. (Acar et al., 2021), (McMahan et al., 2017)

$$\arg \min_{\mathbf{w} \in \mathbb{R}^d} \left( f(\mathbf{w}) \triangleq \frac{1}{K} \sum_{k \in [K]} f_k(\mathbf{w}) \right) \quad (1)$$

where  $f_k(\mathbf{w})$  is the client specific objective function and  $w$  denotes model parameters. The overall FL framework is described in detail in Figure 2.

### 3.2. Adaptive Self-Distillation (ASD) in FL

We now describe the proposed method where each client  $k$  minimizes the  $f_k(\mathbf{w})$ , defined as:

$$f_k(\mathbf{w}) \triangleq L_k(\mathbf{w}) + \lambda L_k^{ASD}(\mathbf{w}) \quad (2)$$

where  $L_k(\mathbf{w})$  is given as:

$$L_k(\mathbf{w}) = \mathbb{E}_{x, y \in P_k(x, y)} [l_k(\mathbf{w}; (x, y))] \quad (3)$$

Here,  $l_k$  is the cross-entropy loss. The expectation is computed over training samples drawn from  $\mathbb{P}_k(x, y)$  of a client  $k$ . This is approximated as the empirical average of the samples from the Dataset  $\mathcal{D}_k$ .

$L_k^{ASD}(\mathbf{w})$  in Eq. 2 denotes the proposed *ASD loss* term which considers label imbalance and quantifies how easily the predictions of the local model can drift from the global model. ASD loss is designed so that client models learn from the local data and at the same time not drift too much from the global model. We define ASD loss as:

$$L_k^{ASD}(\mathbf{w}) \triangleq \mathbb{E}[\alpha_k(x, y) \mathcal{D}_{\text{KL}}(q_g(x, \mathbf{w}^t) || q_k(x, \mathbf{w}))] \quad (4)$$

In the above Eq. 4,  $\mathbf{w}^t$  represents the global model at round  $t$ ,  $\mathbf{w}$  is the trainable model parameters of client  $k$ , and  $\alpha_k(x, y)$  denotes the weight for the sample  $x$  with label ground truth label  $y$ . For simplicity, we denote the global model softmax predictions  $q_g(x, \mathbf{w}^t)$  as  $q_g(x)$  and client model softmax

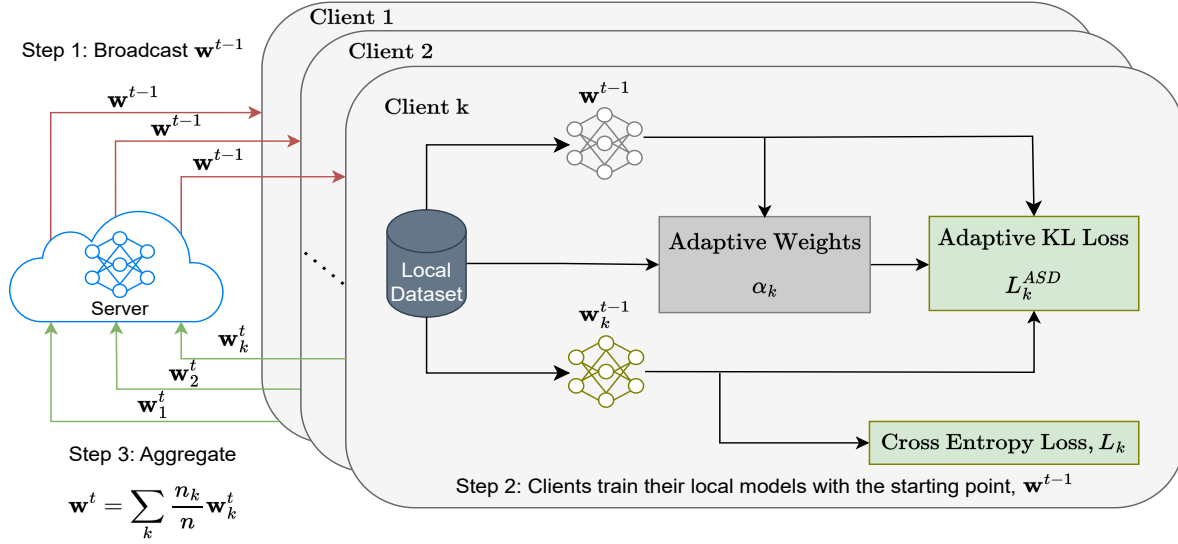


Figure 2. Federated Learning with Adaptive Self-Distillation. The figure describes the overview of the proposed approach based on Adaptive distillation. In **Step 1**, The server broadcasts the model parameters. In **Step 2**, clients train their models by minimizing both the cross entropy loss and predicted probability distribution over the classes between the global model and the client model by minimizing the KL divergence. The importance of the sample in the batch is decided by the proposed adaptive scheme as a function of label distribution and the entropy. The server model is fixed while training the client. In **Step 3**, the server aggregates the client models based on FedAvg aggregation. The process repeats till convergence.

predictions  $q_k(x, \mathbf{w})$  as  $q_k(x)$ .  $\mathcal{D}_{\text{KL}}$  is the KL divergence. Eq. 4 can be approximated for mini-batch training as:

$$L_k^{\text{ASD}}(\mathbf{w}) = \frac{1}{B} \sum_{i \in [B]} \alpha_k(x^i, y^i) \mathcal{D}_{\text{KL}}(q_g(x^i) || q_k(x^i)) \quad (5)$$

where  $B$  is the batch size,  $(x^i, y^i) \in \mathcal{D}_k$  and  $q_g$  and  $q_k$  are softmax probabilities on the temperature ( $\tau$ ) scaled logits of the global model and client model  $k$ , respectively. They are defined as:

$$q_g^c(x^i) = \frac{\exp(z_g^c(x^i)/\tau)}{\sum_{m \in C} \exp(z_g^m(x^i)/\tau)} \quad (6)$$

$$q_k^c(x^i) = \frac{\exp(z_k^c(x^i)/\tau)}{\sum_{m \in C} \exp(z_k^m(x^i)/\tau)} \quad (7)$$

where  $z_g(x^i)$ ,  $z_k(x^i)$  are the logits predicted on the input  $x^i$  by the global model and client model  $k$  respectively. The index  $i$  denotes the  $i^{\text{th}}$  sample of the batch. The  $\mathcal{D}_{\text{KL}}(q_g(x^i) || q_k(x^i))$  is given as:

$$\mathcal{D}_{\text{KL}}(q_g(x^i) || q_k(x^i)) = \sum_{c=1}^C q_g^c(x^i) \log(q_g^c(x^i)/q_k^c(x^i)) \quad (8)$$

where  $C$  is the number of classes. We use the simplified notation  $\alpha_k^i$  for distillation weights  $\alpha_k(x^i, y^i)$ , given as:

$$\alpha_k^i = \frac{\hat{\alpha}_k^i}{\sum_{i \in B} \hat{\alpha}_k^i} \quad (9)$$

and  $\hat{\alpha}_k^i$  is defined as:

$$\hat{\alpha}_k^i \triangleq \frac{\exp(-\mathcal{H}(x^i))}{p_k^{y^i}} \quad (10)$$

where  $\mathcal{H}(x^i)$  is the entropy of the global model predictions, defined as <sup>1</sup>:

$$\mathcal{H}(x^i) = \sum_{c=1}^C -q_g^c(x^i) \log(q_g^c(x^i)) \quad (11)$$

$\mathcal{D}_{\text{KL}}$  in Eq. 8 captures how close the local model's predictions are to the global model for a given sample  $x^i$ . Our weighting scheme in Eq. 11 decides how much to learn from the global model for that sample based on the entropy  $\mathcal{H}(x^i)$  of the server model predictions and the label distribution of the client data ( $p_k^{y^i}$ ).  $\mathcal{H}(x^i)$  captures the confidence of global model predictions. Since a higher value implies that the server predictions are noisy, we tend to reduce the weight, i.e, we give less importance to the global model if its entropy is high.  $p_k^{y^i}$  is the probability that the sample belongs to a particular class. We give more weight to the sample if it belongs to the minority class. This promotes learning from the local data for the classes where the representation is sufficient enough, and for the minority classes we encourage them to stay closer to the global model. We

<sup>1</sup>While computing the entropy we set  $\tau$  to be 1

approximate the label distribution  $p_k^{y^i}$  with the empirical label distribution. It is computed as:

$$p_k^{y^i=c} = \frac{\sum_{i \in |\mathcal{D}_k|} \mathbb{I}_{y^i=c}}{|\mathcal{D}_k|} \quad (12)$$

where  $\mathbb{I}_{y^i=c}$  denotes the indicator function and its value is 1 if the label of the  $i^{\text{th}}$  training sample belongs to class  $c$  else it is 0. To simplify the notation, we use  $p_k^c$  for  $p_k^{y^i=c}$  as it depends only on the class  $c$  for a client  $k$ . Finally we use Eqs. 8 and 11 to compute  $L_k^{\text{ASD}}(\mathbf{w})$ , defined in Eq. 4.

### 3.3. Theoretical Analysis of Gradient Dissimilarity

In this section, we offer the theoretical analysis of client drift. We now introduce *gradient dissimilarity*  $G_d$  based on the works of (Li et al., 2020; Lee et al., 2022) as a way to measure the extent of client-drift as:

$$G_d(\mathbf{w}, \lambda) = \frac{\frac{1}{K} \sum_k \|\nabla f_k(\mathbf{w})\|^2}{\|\nabla f(\mathbf{w})\|^2} \quad (13)$$

$G_d(\mathbf{w}, \lambda)$  is function of both the  $\mathbf{w}$  and  $\lambda$ . For convenience, we simply write  $G_d$  and mention arguments explicitly when required.  $f_k(\mathbf{w})$  in the above Eq. 13 is the same as Eq. 2. With this, we now establish a series of propositions to show that ASD regularization reduces the gradient dissimilarity which leads to lower client drift.

**Proposition 3.1.**  $\inf_{\mathbf{w} \in \mathbb{R}^d} G_d(\mathbf{w}, \lambda)$  is 1,  $\forall \lambda$

The above proposition implies that if all the client’s gradients are progressing in the same direction, which means there is no drift  $G_d = 1$ . The result follows from Jensen’s inequality. The lower value of  $G_d$  is desirable and ideally 1. To analyze the  $G_d$ , we need  $\nabla f_k(\mathbf{w})$  which is given in the below proposition.

**Proposition 3.2.** *When the class conditional distribution across the clients is identical, i.e.,  $\mathbb{P}_k(x | y) = \mathbb{P}(x | y)$  then  $\nabla f_k(\mathbf{w}) = \sum_c p_k^c (\mathbf{g}_c + \lambda \gamma_k^c \tilde{\mathbf{g}}_c)$ , where  $\mathbf{g}_c = \nabla \mathbb{E}[l(\mathbf{w}; x, y) | y = c]$ ,  $\tilde{\mathbf{g}}_c = \nabla \mathbb{E}[\exp(-\mathcal{H}(x)) \mathcal{D}_{\text{KL}}(q_g(x) | q_k(x)) | y = c]$  and  $\gamma_k^c = \frac{1}{p_k^c}$ .*

The result follows from the tower property of expectation and the assumption that class conditional distribution is the same for all the clients. From the above proposition, we can see that the gradients  $\nabla f_k(\mathbf{w})$  only differ due to  $p_k^c$  which captures the data heterogeneity due to label imbalance. The proof is given in Section I of the Appendix.

**Assumption 3.3.** Class-wise gradients are weakly correlated and similar magnitude  $\mathbf{g}_c^\top \mathbf{g}_c \ll \mathbf{g}_c^\top \mathbf{g}_m$ ,  $\tilde{\mathbf{g}}_c^\top \tilde{\mathbf{g}}_c \ll \tilde{\mathbf{g}}_c^\top \tilde{\mathbf{g}}_m$  and for  $c \neq m$

The assumption on weakly correlated class-wise gradients intuitively implies that gradients of loss for a specific class cannot give any significant information on the gradients of the other class.

**Proposition 3.4.** *When the class-conditional distribution across the clients is the same, and the Assumption 3.3 holds then  $\exists$  a range of values for  $\lambda$  such that whenever  $\lambda \geq \lambda_c$  we have  $\frac{dG_d}{d\lambda} < 0$  and  $G_d(\mathbf{w}, \lambda) < G_d(\mathbf{w}, 0)$ .*

The proposition implies that there is a value of  $\lambda \geq \lambda_c$  such that the derivative of  $G_d$  w.r.t  $\lambda$  is negative. The proof is given in Section I of the Appendix. This indicates that by appropriately selecting the value of  $\lambda$  we can make  $G_d$  lower, which in turn reduces the client drift. One of the key assumptions on the heterogeneity is the existence of the following quantity:

$$B^2(\lambda) := \sup_{\mathbf{w} \in \mathbb{R}^d} G_d(\mathbf{w}, \lambda) \quad (14)$$

which leads to the following assumption:

**Assumption 3.5.**  $\frac{1}{K} \sum_k \|\nabla f_k(\mathbf{w})\|^2 \leq B^2(\lambda) \|\nabla f(\mathbf{w})\|^2$

This is the bounded gradient dissimilarity assumption used in (Li et al., 2020). Next, we show the existence of  $\lambda$  such that  $B^2(\lambda) < B^2(0)$ , which means that with the regularizer we can tightly bound the gradient dissimilarity compared to the case without the regularizer, i.e., ( $\lambda = 0$ ).

**Proposition 3.6.** *Suppose the functions  $f_k$  satisfy Assumption 3.5 above then we have  $B^2(\lambda) < B^2(0)$ .*

*Proof.* From 14 we have

$$B^2(\lambda) = \sup_{\mathbf{w} \in \mathbb{R}^d} G_d(\mathbf{w}, \lambda) \quad (15)$$

For a fixed  $\lambda$  as per Proposition 3.4 we have the following.

$$\sup_{\mathbf{w} \in \mathbb{R}^d} G_d(\mathbf{w}, \lambda) < \sup_{\mathbf{w} \in \mathbb{R}^d} G_d(\mathbf{w}, 0) \quad (16)$$

The above inequality Eq. 16 is true as Proposition 3.4 guarantees that the value of  $G_d(\mathbf{w}, \lambda) < G_d(\mathbf{w}, 0)$  for all  $\mathbf{w}$  when  $\lambda \geq \lambda_c$ . If inequality Eq. 16 is not true, then one can find a  $\mathbf{w}$  that contradicts the Proposition 3.4, which is impossible. This means for some value of  $\lambda \geq \lambda_c$  we have  $B^2(\lambda) < B^2(0)$  from Eq. 14 and Eq. 16.  $\square$

The key takeaway from this analysis is that by introducing the regularizer we can tightly bound the heterogeneity when compared to the case without the regularizer. *Based on the*

works (Karimireddy et al., 2020; Li et al., 2020) we explain that a lower  $B^2(\lambda)$  implies better convergence. More details are provided in the Section J of the Appendix.

### 3.4. Discussion on the Generalization of ASD

The key reason for better generalization is the adaptive self-distillation loss. It has been shown in (Mobahi et al., 2020) that self-distillation improves the generalization in centralized settings. It has also been empirically shown in (Zhang et al., 2019) that self-distillation helps the model to converge to a flat minimum. Generally, converging to flat minimum is indicative of improved generalization, a concept explored in prior studies (Keskar et al., 2017; Yao et al., 2020). The top eigenvalue and the trace of the Hessian computed from the training loss are typical measures of ‘flatness’ of the minimum to which the training converges, i.e., lower values of these measures indicate the presence of a flat minimum. To gain a deeper understanding of this phenomenon in a federated learning setting, we analyze the top eigenvalue and the trace of the Hessian of the cross-entropy loss for global models obtained with and without the ASD regularizer. The following argument establishes that if the client models converge to flat minimum, it would also ensure convergence of the resultant global model to a flat minimum. We assume the Hessians of the functions  $f_k$  ( $k^{th}$  client’s local objective),  $f$  (resultant global objective) exist and are continuous. Since  $f = \frac{1}{K} \sum_{i=1}^K f_i$ , we have  $\mathbf{H}(f) = \frac{1}{K} \sum_{i=1}^K \mathbf{H}(f_i)$  ( $\mathbf{H}(g)$  denotes the Hessian of function  $g$ ). This implies  $\mu_1(\mathbf{H}(f)) \leq \frac{1}{K} \sum_{i=1}^K \mu_1(\mathbf{H}(f_i))$  ( $\mu_1(\mathbf{A})$  denotes top eigenvalue of matrix  $\mathbf{A}$ ). Thus when the local models converge to a flat minimum, it will ensure the convergence of the global model to a flat minimum. Following the method of (Yao et al., 2020), we computed the top eigenvalue and trace of the Hessian. In Table 1, we observe that FedAvg+ASD attains lower values for the top eigenvalue and trace compared to FedAvg, suggesting convergence to flat minimum. The Eigen density plot in the figure 3 also confirms the same. A similar concept has been explored in FedSAM (Qu et al., 2022; Caldarola et al., 2022). But the issue with SAM-based methods is that they require an extra forward and backward pass which doubles the computation cost of the edge devices. However, our method can be applied to SAM-based methods and further improve its performance. ASD consistently attains the flatness with the other FL algorithms and enhances their generalization, these are described in Section H of the Appendix.

## 4. Experiments

We perform the experiments on CIFAR-10, CIFAR-100 dataset (Krizhevsky & Hinton, 2009), Tiny-ImageNet (Le & Yang, 2015) dataset with different degrees of heterogeneity in the balanced settings (i.e., the same number of samples per client but the class label distribution of each varies). We

Table 1. Hessian Analysis on the converged models obtained using FedAvg and FedAvg + ASD on CIFAR-100 dataset.

Method	Top Eigenvalue ↓	Trace ↓
FedAvg	53.6	8516
FedAvg + ASD	<b>12.33</b>	<b>2269</b>

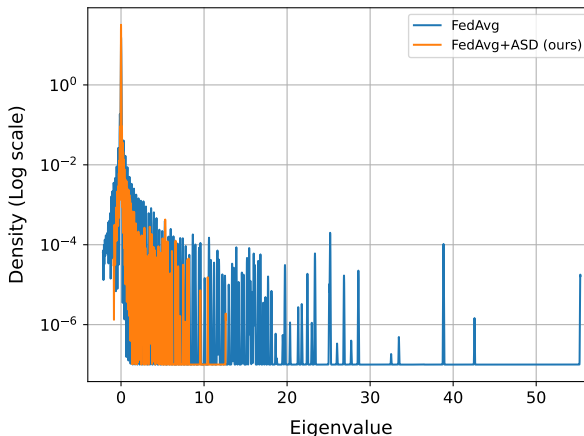


Figure 3. Eigen spectrum with and without the ASD regularizer. It is evident that ASD regularizer minimizes most of the eigenvalues along with the top eigenvalue and attains flatness.

set the total number of clients to 100 in all our experiments. We sample the clients with a ratio of 0.1, i.e., 10 percent of clients are sampled on an average per communication round, similar to the protocol followed in (Acar et al., 2021). We build our experiments using publicly available codebase by (Acar et al., 2021). For generating non-iid data, Dirichlet distribution is used. To simulate the effect of label imbalance, for every client we sample the ‘probability distribution’ over the classes from the distribution  $p_k^{dir} = Dir(\delta, C)$ . Every sample of  $p_k^{dir}$  is a vector of length  $C$  and all the elements of this vector are non-negative and sum to 1. This vector represents the label distribution for the client. The parameter  $\delta$  captures the degree of heterogeneity. Lower values of  $\delta$  capture high heterogeneity and as the value of  $\delta$  increases, the label distribution becomes more uniform. Another parameter of Dirichlet distribution (i.e.,  $C$ ), its value can be interpreted from the training dataset ( $C = 100$  for CIFAR-100). For notational convenience, we omit  $C$  from  $Dir(\delta, C)$  by simply re-writing as  $Dir(\delta)$ . By configuring the concentration parameter  $\delta$  to 0.6 and 0.3, we generate the data from moderate to high heterogeneity, which is in line with the approach followed in (Acar et al., 2021) and (Yurochkin et al., 2019). In a balanced setting, each client receives the same number of samples.

Table 2. Comparison of Accuracy(%): We show the accuracy attained by the algorithms across the datasets (CIFAR-100/Tiny-ImageNet) at the end of 500 communication rounds. It can be seen that by combining the proposed approach the performance of all the algorithms can be significantly improved.

Algorithm	CIFAR-100			TinyImageNet		
	$\delta = 0.3$	$\delta = 0.6$	IID	$\delta = 0.3$	$\delta = 0.6$	IID
FedAvg (McMahan et al., 2017)	38.67 $\pm$ 0.66	38.53 $\pm$ 0.32	37.68 $\pm$ 0.41	23.89 $\pm$ 0.84	23.95 $\pm$ 0.72	23.48 $\pm$ 0.61
FedAvg+ASD (Ours)	<b>42.77</b> $\pm$ 0.22	<b>42.54</b> $\pm$ 0.51	<b>43.00</b> $\pm$ 0.60	<b>25.31</b> $\pm$ 0.25	<b>26.38</b> $\pm$ 0.21	<b>26.67</b> $\pm$ 0.10
FedProx (Li et al., 2020)	37.79 $\pm$ 0.97	37.92 $\pm$ 0.55	37.94 $\pm$ 0.22	24.61 $\pm$ 1.24	23.57 $\pm$ 0.44	23.27 $\pm$ 0.11
FedProx+ASD (Ours)	<b>41.31</b> $\pm$ 0.90	<b>41.67</b> $\pm$ 0.12	<b>42.30</b> $\pm$ 0.37	<b>25.49</b> $\pm$ 0.45	<b>25.62</b> $\pm$ 0.05	<b>25.58</b> $\pm$ 0.18
FedNTD (Lee et al., 2022)	40.40 $\pm$ 1.52	40.50 $\pm$ 0.54	41.23 $\pm$ 0.44	23.71 $\pm$ 0.65	23.28 $\pm$ 0.29	22.95 $\pm$ 0.22
FedNTD+ASD (Ours)	<b>43.01</b> $\pm$ 0.34	<b>43.61</b> $\pm$ 0.33	<b>43.25</b> $\pm$ 0.41	<b>27.34</b> $\pm$ 0.73	<b>27.39</b> $\pm$ 0.39	<b>27.41</b> $\pm$ 0.11
FedDyn (Acar et al., 2021)	47.29 $\pm$ 0.41	48.60 $\pm$ 0.09	48.87 $\pm$ 0.51	27.62 $\pm$ 0.21	28.58 $\pm$ 0.61	28.37 $\pm$ 0.20
FedDyn+ASD (Ours)	<b>48.41</b> $\pm$ 0.36	<b>50.23</b> $\pm$ 0.25	<b>51.44</b> $\pm$ 0.48	<b>29.94</b> $\pm$ 0.67	<b>30.05</b> $\pm$ 0.24	<b>30.76</b> $\pm$ 0.44
FedSAM (Caldarola et al., 2022)	40.89 $\pm$ 0.30	41.41 $\pm$ 0.34	40.81 $\pm$ 0.26	24.72 $\pm$ 0.64	25.42 $\pm$ 0.49	23.50 $\pm$ 0.94
FedSAM+ASD (Ours)	<b>43.99</b> $\pm$ 0.14	<b>44.54</b> $\pm$ 0.30	<b>44.77</b> $\pm$ 0.11	<b>26.26</b> $\pm$ 0.47	<b>26.80</b> $\pm$ 0.17	<b>25.37</b> $\pm$ 0.26
FedDisco (Ye et al., 2023)	38.97 $\pm$ 1.38	38.87 $\pm$ 1.37	37.85 $\pm$ 0.57	24.35 $\pm$ 0.42	24.03 $\pm$ 0.78	23.49 $\pm$ 0.31
FedDisco+ASD (Ours)	<b>41.55</b> $\pm$ 1.06	<b>41.94</b> $\pm$ 0.30	<b>43.09</b> $\pm$ 0.47	<b>25.43</b> $\pm$ 0.46	<b>26.03</b> $\pm$ 0.26	<b>26.56</b> $\pm$ 0.9
FedSpeed (Sun et al., 2023)	47.39 $\pm$ 0.82	48.27 $\pm$ 0.13	49.01 $\pm$ 0.46	28.60 $\pm$ 0.15	29.33 $\pm$ 0.3	29.62 $\pm$ 0.31
FedSpeed+ASD (Ours)	<b>49.16</b> $\pm$ 0.40	<b>49.76</b> $\pm$ 0.27	<b>51.99</b> $\pm$ 0.32	<b>30.97</b> $\pm$ 0.25	<b>30.05</b> $\pm$ 0.24	<b>32.68</b> $\pm$ 0.53

## 5. Results and Discussion

For evaluation, we report accuracy on the test dataset as our performance metric and the number of communication rounds required to attain the desired accuracy as a metric to quantify the communication cost. Specifically, we evaluate the global model on the test set and report its accuracy after every communication round. For comparison, we consider the popular methods for federated learning such as FedAvg, FedProx, FedDyn, FedSpeed, FedNTD, FedSAM and FedDisco. We augment each of these methods with our approach (ASD) and observe a significant boost in performance. For a fair comparison, we consider the same models used in Fedavg (McMahan et al., 2017), and FedDyn (Acar et al., 2021), for CIFAR-10 and CIFAR-100 classification tasks. The model architecture used for CIFAR-100 contains 2 convolution layers followed by 3 fully connected layers. For Tiny-ImageNet, we use 3 convolution followed by 3 fully connected layers. The detailed architectures are given in Sec D of the Appendix. Hyperparameters: SGD algorithm with a learning rate of 0.1 and decay the learning rate per round of 0.998 is used to train the client models. Temperature  $\tau$  is set to 2.0. We only tune the hyper-parameter  $\lambda$ . More hyperparameter details are provided in the Section B of the Appendix. We compare the convergence of different schemes for 500 communication rounds. Following the testing protocol of (Acar et al., 2021), we average across all the client models and compute the test accuracy on the averaged model, which is reported in our results. In all the tables,

we report the test accuracy of the global model in % at the end of 500 communication rounds. All the experiments in the tables are performed over three different initializations, mean and standard deviations of accuracy over the three experiments are reported.

### 5.1. Performance of ASD on CIFAR-10/100 and Tiny-Imagenet

In Table 2, we report the performance of CIFAR-100 and Tiny-ImageNet datasets with various algorithms for non-iid ( $Dir(\delta = 0.3)$  and  $Dir(\delta = 0.6)$ ) and the iid settings. Each experiment is performed over 3 different initializations, and the mean and standard deviation of the accuracy is reported. The test accuracy vs communication rounds plot on CIFAR-100 dataset is shown in Figure 4. We observe that our proposed ASD applied on FedDyn improves its performance by  $\approx 1.1\%$  for  $Dir(\delta = 0.3)$  and  $\approx 1.6\%$   $Dir(\delta = 0.6)$ . We can see that adding ASD gives consistent improvement across the rounds<sup>2</sup>. A similar plot for Tiny-Imagenet dataset is shown in Figure 5. We observe that FedDyn+ASD improves FedDyn by  $\approx 1.4\%$  for  $Dir(\delta = 0.3)$  and by  $\approx 2.4\%$  for  $Dir(\delta = 0.6)$ . We obtain significant improvements for FedAvg+ASD against FedAvg, FedProx+ASD against FedProx, FedSpeed+ASD

<sup>2</sup>In the figures we only compare FedAvg, FedDyn and FedSpeed for better readability. For others please refer to Sec F of the Appendix

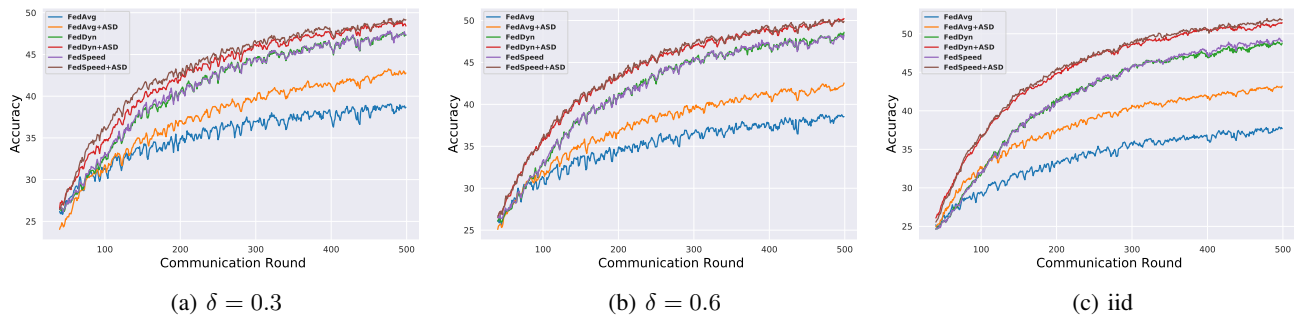


Figure 4. Test Accuracy vs Communication rounds: Comparison of algorithms with  $\delta = 0.3$ ,  $\delta = 0.6$  and iid data partitions on CIFAR-100 dataset. All the algorithms augmented with proposed regularization (ASD) outperform compared to their original form.

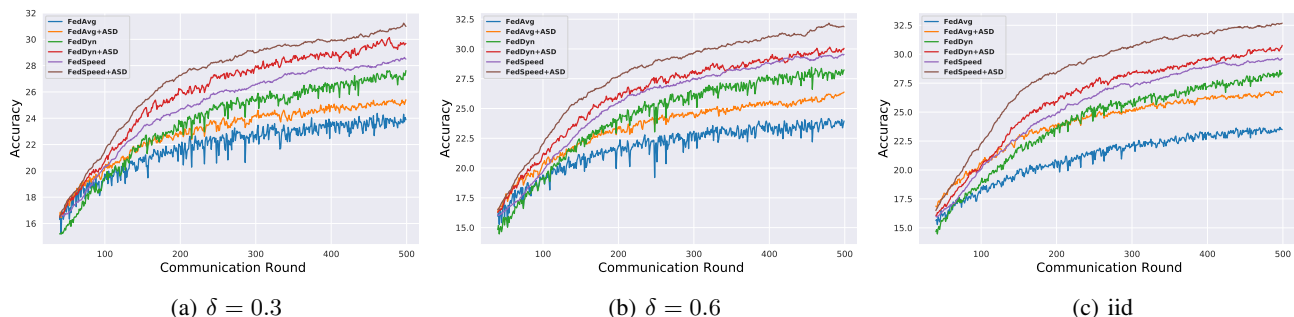


Figure 5. Test Accuracy vs Communication rounds: Comparison of algorithms with  $\delta = 0.3$ ,  $\delta = 0.6$  and iid data partitions on Tiny-ImageNet dataset. All the algorithms augmented with proposed regularization (ASD) outperform compared to their original form.

against FedSpeed, etc. In Sec C of the Appendix we present the CIFAR-10 results where we observe that adding ASD consistently gives an improvement of  $\approx 0.7\% - 0.8\%$  improvement across all the algorithms. Further ablations are provided in Section E of the Appendix.

## 6. Computation Cost

The major computation for the distillation scheme comes from the teacher forward pass, student forward pass, and the student backward pass (Xu et al., 2020). If we assume  $C_s$  as the total computational cost of server forward pass and  $C_k$  be the total computation cost of client model  $k$  the forward pass per epoch. We do not need  $C_s$  computations every epoch, we only need to compute once and store the values of  $\mathcal{H}(x)$ . For the computation of distillation regularizer we only need  $E * C_k + C_s$  local computations. Since  $C_s = C_k$ , we have  $(E + 1) * C_k$  local computations. Thus our regularizer introduces minimal computation on the edge devices which typically have low compute.

## 7. Conclusion

We presented an efficient and effective method for addressing data heterogeneity due to label imbalance in Federated learning using Adaptive Self-Distillation (ASD), which does not require any auxiliary data and no extra communication cost. We also theoretically showed that ASD has lower client-drift leading to better convergence. Moreover, we also performed analysis to show that ASD has better generalization by analyzing Hessian’s top eigenvalue and trace. The effectiveness of our approach is shown via extensive experiments across datasets such as CIFAR-10, CIFAR-100 and Tiny-ImageNet with different degrees of heterogeneity. Our proposed approach to ASD can be integrated easily into any of the FL frameworks. We showed its efficacy by improving the performance when combined with FedAvg, FedProx, FedDyn, FedSAM, FedDisco, FedNTD and FedSpeed. Our research can inspire the designing of the regularizers that concurrently reduce client-drift and improve the generalization.



---

## References

- Acar, D. A. E., Zhao, Y., Navarro, R. M., Mattina, M., Whatmough, P. N., and Saligrama, V. Federated learning based on dynamic regularization. *arXiv preprint arXiv:2111.04263*, 2021.
- Caldarola, D., Caputo, B., and Ciccone, M. Improving generalization in federated learning by seeking flat minima. In *European Conference on Computer Vision*, pp. 654–672. Springer, 2022.
- Geiping, J., Bauermeister, H., Dröge, H., and Moeller, M. Inverting gradients-how easy is it to break privacy in federated learning? *Advances in Neural Information Processing Systems*, 33:16937–16947, 2020.
- Hard, A., Kiddon, C. M., Ramage, D., Beaufays, F., Eichner, H., Rao, K., Mathews, R., and Augenstein, S. Federated learning for mobile keyboard prediction, 2018. URL <https://arxiv.org/abs/1811.03604>.
- He, Y., Chen, Y., Yang, X., Yu, H., Huang, Y.-H., and Gu, Y. Learning critically: Selective self-distillation in federated learning on non-iid data. *IEEE Transactions on Big Data*, pp. 1–12, 2022a. doi: 10.1109/TBDATA.2022.3189703.
- He, Y., Chen, Y., Yang, X., Zhang, Y., and Zeng, B. Class-wise adaptive self distillation for heterogeneous federated learning. 2022b.
- Hinton, G., Vinyals, O., Dean, J., et al. Distilling the knowledge in a neural network. *arXiv preprint arXiv:1503.02531*, 2(7), 2015.
- Hsu, T.-M. H., Qi, H., and Brown, M. Federated visual classification with real-world data distribution. In *Computer Vision—ECCV 2020: 16th European Conference, Glasgow, UK, August 23–28, 2020, Proceedings, Part X 16*, pp. 76–92. Springer, 2020.
- Huang, Y., Gupta, S., Song, Z., Li, K., and Arora, S. Evaluating gradient inversion attacks and defenses in federated learning. *Advances in Neural Information Processing Systems*, 34:7232–7241, 2021.
- Kairouz, P., McMahan, H. B., Avent, B., Bellet, A., Bennis, M., Bhagoji, A. N., Bonawitz, K., Charles, Z., Cormode, G., Cummings, R., et al. Advances and open problems in federated learning. *Foundations and Trends® in Machine Learning*, 14(1–2):1–210, 2021.
- Karimireddy, S. P., Kale, S., Mohri, M., Reddi, S., Stich, S., and Suresh, A. T. Scaffold: Stochastic controlled averaging for federated learning. In *International Conference on Machine Learning*, pp. 5132–5143. PMLR, 2020.
- Keskar, N. S., Mudigere, D., Nocedal, J., Smelyanskiy, M., and Tang, P. T. P. On large-batch training for deep learning: Generalization gap and sharp minima. In *International Conference on Learning Representations*, 2017. URL <https://openreview.net/forum?id=H1oyRlYgg>.
- Krizhevsky, A. and Hinton, G. Learning multiple layers of features from tiny images. Technical report, Canadian Institute for Advanced Research, 2009.
- Le, Y. and Yang, X. Tiny imagenet visual recognition challenge. *CS 231N*, 7(7):3, 2015.
- Lee, G., Jeong, M., Shin, Y., Bae, S., and Yun, S.-Y. Preservation of the global knowledge by not-true distillation in federated learning. In Oh, A. H., Agarwal, A., Belgrave, D., and Cho, K. (eds.), *Advances in Neural Information Processing Systems*, 2022. URL <https://openreview.net/forum?id=qw3MZblJuo>.
- Li, T., Sahu, A. K., Zaheer, M., Sanjabi, M., Talwalkar, A., and Smith, V. Federated optimization in heterogeneous networks. *Proceedings of Machine Learning and Systems*, 2:429–450, 2020.
- Lin, T., Kong, L., Stich, S. U., and Jaggi, M. Ensemble distillation for robust model fusion in federated learning. *Advances in Neural Information Processing Systems*, 33: 2351–2363, 2020.
- McMahan, B., Moore, E., Ramage, D., Hampson, S., and y Arcas, B. A. Communication-efficient learning of deep networks from decentralized data. In *Artificial intelligence and statistics*, pp. 1273–1282. PMLR, 2017.
- Mishchenko, K., Gorbunov, E., Takáč, M., and Richtárik, P. Distributed learning with compressed gradient differences. *arXiv preprint arXiv:1901.09269*, 2019.
- Mobahi, H., Farajtabar, M., and Bartlett, P. Self-distillation amplifies regularization in hilbert space. *Advances in Neural Information Processing Systems*, 33:3351–3361, 2020.
- Qu, Z., Li, X., Duan, R., Liu, Y., Tang, B., and Lu, Z. Generalized federated learning via sharpness aware minimization. In *International Conference on Machine Learning*, pp. 18250–18280. PMLR, 2022.
- Ramaswamy, S., Mathews, R., Rao, K., and Beaufays, F. Federated learning for emoji prediction in a mobile keyboard. *arXiv preprint arXiv:1906.04329*, 2019.
- Rieke, N., Hancox, J., Li, W., Milletari, F., Roth, H. R., Albarqouni, S., Bakas, S., Galtier, M. N., Landman, B. A., Maier-Hein, K., et al. The future of digital health with federated learning. *NPJ digital medicine*, 3(1):1–7, 2020.

- 
- Seo, H., Park, J., Oh, S., Bennis, M., and Kim, S.-L. 16 federated knowledge distillation. *Machine Learning and Wireless Communications*, pp. 457, 2022.
- Stich, S. U. Local sgd converges fast and communicates little. *arXiv preprint arXiv:1805.09767*, 2018.
- Sun, Y., Shen, L., Huang, T., Ding, L., and Tao, D. Fed-speed: Larger local interval, less communication round, and higher generalization accuracy. In *The Eleventh International Conference on Learning Representations*, 2023. URL <https://openreview.net/forum?id=bZjxxYURKT>.
- Tang, S., Feng, L., Shao, W., Kuang, Z., Zhang, W., and Chen, Y. Learning efficient detector with semi-supervised adaptive distillation. *arXiv preprint arXiv:1901.00366*, 2019.
- Wang, J., Charles, Z., Xu, Z., Joshi, G., McMahan, H. B., Al-Shedivat, M., Andrew, G., Avestimehr, S., Daly, K., Data, D., et al. A field guide to federated optimization. *arXiv preprint arXiv:2107.06917*, 2021.
- Xu, G., Liu, Z., and Loy, C. C. Computation-efficient knowledge distillation via uncertainty-aware mixup. *arXiv preprint arXiv:2012.09413*, 2020.
- Xu, J., Glicksberg, B. S., Su, C., Walker, P., Bian, J., and Wang, F. Federated learning for healthcare informatics. *Journal of Healthcare Informatics Research*, 5:1–19, 2021.
- Yadav, S. and Yadav, R. S. A review on energy efficient protocols in wireless sensor networks. *Wireless Networks*, 22(1):335–350, 2016.
- Yao, Z., Gholami, A., Keutzer, K., and Mahoney, M. W. Pyhessian: Neural networks through the lens of the hessian. In *2020 IEEE international conference on big data (Big data)*, pp. 581–590. IEEE, 2020.
- Ye, R., Xu, M., Wang, J., Xu, C., Chen, S., and Wang, Y. Feddisco: Federated learning with discrepancy-aware collaboration. 2023.
- Yurochkin, M., Agarwal, M., Ghosh, S., Greenewald, K., Hoang, N., and Khazaeni, Y. Bayesian nonparametric federated learning of neural networks. In *International Conference on Machine Learning*, pp. 7252–7261. PMLR, 2019.
- Zhang, J., Li, Z., Li, B., Xu, J., Wu, S., Ding, S., and Wu, C. Federated learning with label distribution skew via logits calibration. In *International Conference on Machine Learning*, pp. 26311–26329. PMLR, 2022.
- Zhang, L., Song, J., Gao, A., Chen, J., Bao, C., and Ma, K. Be your own teacher: Improve the performance of convolutional neural networks via self distillation. In *Proceedings of the IEEE/CVF international conference on computer vision*, pp. 3713–3722, 2019.
- Zhang, X., Hong, M., Dhople, S., Yin, W., and Liu, Y. Fedpd: A federated learning framework with optimal rates and adaptivity to non-iid data. *arXiv preprint arXiv:2005.11418*, 2020.
- Zhou, Y., Pu, G., Ma, X., Li, X., and Wu, D. Distilled one-shot federated learning. *arXiv preprint arXiv:2009.07999*, 2020.
- Zhu, Z., Hong, J., and Zhou, J. Data-free knowledge distillation for heterogeneous federated learning. In *International Conference on Machine Learning*, pp. 12878–12889. PMLR, 2021.

---

## A. Notations and Definitions

- $\mathcal{H}(x)$  denotes the entropy of the model under consideration for input  $x$ .
- $p_k^{y^i=c}$  denotes the probability that the client  $k$  has the input  $i$  belonging to class  $c$ .
- $\mathbf{H}(g)$  denotes the Hessian of the function  $g$ .
- $\mu_1(\mathbf{A})$  denotes the top eigenvalue of matrix  $\mathbf{A}$ .
- $\mathcal{D}_{KL}$  denotes the KL divergence.
- $\inf$  denotes the infimum and  $\sup$  denotes the supremum.
- $\delta$  is used for denoting the heterogeneity generated based on Dirichlet distribution.
- $\lambda$  denotes the ASD regularizer strength.
- $G_d(\mathbf{w}, \lambda)$  denotes the gradient dissimilarity.
- $\mathbb{E}(\cdot)$  denotes the expectation.
- $L_k(\mathbf{w})$  is the loss of client  $k$  (cross-entropy loss).
- $L_k(\mathbf{w})^{ASD}$  is the Adaptive Self-Distillation loss for client  $k$ .
- $\mathcal{D}_k$  represents the dataset of client  $k$ .
- $\mathcal{P}_k(x, y)$  represents the data distribution of the client  $k$ .

## B. Hyper-Parameter Settings

We chose  $\lambda$  from  $\{10, 20, 30\}$ . We set  $\lambda = 20$  for all the Tiny-ImageNet experiments. For CIFAR-10/100 we chose  $\lambda$  to be 10 and 20 respectively. Batch-size of 50 and learning rate of 0.1 with decay of 0.998 is employed for all the experiments. All the experiments are carried out with 100 clients and with 10% client participation rate.

### B.1. Sensitivity to hyperparameters $\lambda$

We study the impact of changing the hyper-parameter on the CIFAR-100 dataset with the Dirichlet non-iid partition of  $\delta = 0.3$ . When using FedAvg+ASD algorithm. In Figure 6 we see that the accuracy of the model increases with  $\lambda$  and then drops after a critical point.

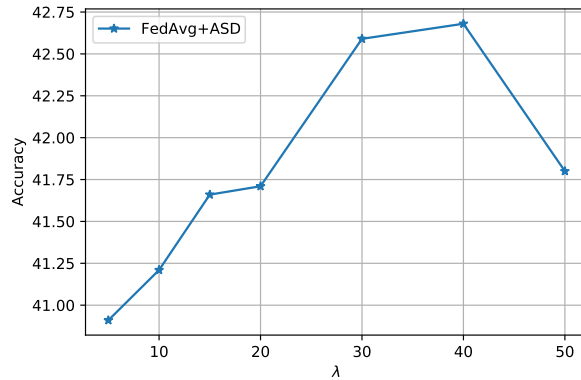


Figure 6. Study of hyper-parameter’s sensitivity for CIFAR-100 and  $\delta = 0.3$  with FedAvg+ASD. Accuracy is sensitive at lower values of  $\lambda$ .

Table 3. We show the accuracy attained by the algorithms on CIFAR-10 at the end of 500 communication rounds. It can be seen that by combining the proposed approach the performance of all the algorithms is improved.

Algorithm	$\delta = 0.3$	$\delta = 0.6$	iid
FedAvg	78.15 $\pm$ 0.78	78.66 $\pm$ 0.10	80.99 $\pm$ 0.09
FedAvg+ASD ( <b>Ours</b> )	<b>79.01</b> $\pm$ 0.33	<b>79.93</b> $\pm$ 0.21	<b>81.83</b> $\pm$ 0.19
FedProx	78.25 $\pm$ 0.68	78.81 $\pm$ 0.69	81.04 $\pm$ 0.34
FedProx+ASD ( <b>Ours</b> )	<b>78.77</b> $\pm$ 0.49	<b>79.91</b> $\pm$ 0.12	<b>81.74</b> $\pm$ 0.06
FedNTD	76.79 $\pm$ 0.37	78.55 $\pm$ 0.31	80.98 $\pm$ 0.21
FedNTD+ASD ( <b>Ours</b> )	<b>78.78</b> $\pm$ 0.86	<b>80.13</b> $\pm$ 0.49	<b>81.80</b> $\pm$ 0.11
FedDyn	81.08 $\pm$ 0.52	81.48 $\pm$ 0.35	83.51 $\pm$ 0.27
FedDyn+ASD ( <b>Ours</b> )	<b>81.82</b> $\pm$ 0.56	<b>82.33</b> $\pm$ 0.39	<b>84.09</b> $\pm$ 0.15
FedDisco	78.21 $\pm$ 0.45	78.76 $\pm$ 0.32	81.04 $\pm$ 0.30
FedDisco+ASD ( <b>Ours</b> )	<b>78.97</b> $\pm$ 0.01	<b>79.98</b> $\pm$ 0.35	<b>81.71</b> $\pm$ 0.21
FedSpeed	81.28 $\pm$ 0.32	81.83 $\pm$ 0.36	83.67 $\pm$ 0.14
FedSpeed+ASD ( <b>Ours</b> )	<b>81.70</b> $\pm$ 0.20	<b>82.62</b> $\pm$ 0.26	<b>84.57</b> $\pm$ 0.24

### C. Performance on CIFAR-10 dataset

#### D. Model Architectures

In Table 4, the model architecture is shown. We use PyTorch style representation. For example conv layer(3,64,5) means 3 input channels, 64 output channels and the kernel size is 5. Maxpool(2,2) represents the kernel size of 2 and a stride of 2. FullyConnected(384,200) represents an input dimension of 384 and an output dimension of 200. The architecture for CIFAR-100 is exactly the same as used in (Acar et al., 2021).

CIFAR-10/100 Model	Tiny-ImageNet Model
	ConvLayer(3,64,3)
	GroupNorm(4,64)
	Relu
	MaxPool(2,2)
	ConvLayer(64,64,3)
	GroupNorm(4,64)
ConvLayer(3,64,5)	Relu
Relu	MaxPool(2,2)
MaxPool(2,2)	ConvLayer(64,64,3)
ConvLayer(64,64,5)	GroupNorm(4,64)
Relu	Relu
MaxPool(2,2)	MaxPool(2,2)
Flatten	Flatten
FullyConnected(1600,384)	FullyConnected(4096,512)
Relu	Relu
FullyConnected(384,192)	FullyConnected(512,384)
Relu	Relu
FullyConnected(192,100)	FullyConnected(384,200)

Table 4. Models used for Tiny-ImageNet and CIFAR-100 datasets.

## E. Impact of $\mathcal{H}(x)$ and the $p_k^{y^i}$

We analyze the contribution of KL term for FedAvg+ASD algorithm on the CIFAR-100 dataset with  $Dir(\delta = 0.3)$  non-iid data partition. In table 5, we analyze the contribution of each term. It can be seen that both significantly contribute, and when both are used, it further leads to improved performance. All the accuracies are reported by averaging over three different initializations.

Table 5. Ablation study on CIFAR-100 datasets

Algorithm	$\mathcal{H}(x)$	$p_k^{y^i}$	Accuracy CIFAR-100
FedAvg	NA	NA	38.67 $\pm$ 0.66
FedAvg+ASD	✓	✗	42.35 $\pm$ 0.26
FedAvg+ASD	✗	✓	42.12 $\pm$ 0.30
FedAvg+ASD	✓	✓	42.77 $\pm$ 0.22

### E.1. Comparison with adaptive vs uniform weights

Table 6. Comparison with adaptive weights vs uniform weights on CIFAR-100 dataset

Data partition	Self-Distillation with Uniform weights	Self-Distillation with Adaptive weights
$\delta = 0.3$	41.75 $\pm$ 0.12	42.77 $\pm$ 0.22
$\delta = 0.6$	41.69 $\pm$ 0.20	42.54 $\pm$ 0.51

We analyze the impact of the proposed adaptive weighting scheme. We compare by making all the alpha values in Eq 10 to 1. We can see from Table 6 that in the non-iid scenarios, the proposed adaptive weighting scheme is better than assigning the uniform weights, thus establishing the impact of proposed adaptive weights.

## F. Accuracy vs Communication rounds

In the below figures, we present how the Accuracy is evolving across the communication rounds for the remaining algorithms.

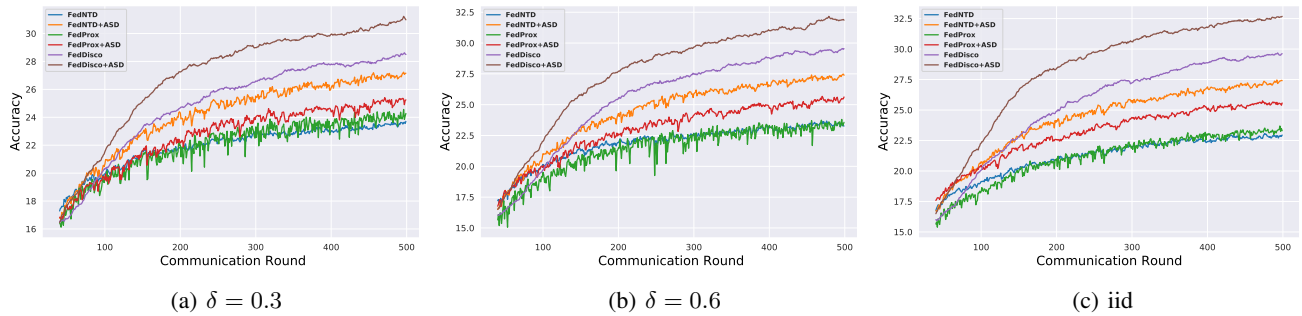


Figure 7. Test Accuracy vs Communication rounds: Comparison of algorithms with  $\delta = 0.3$ ,  $\delta = 0.6$  and iid data partitions on Tiny-ImageNet dataset. All the algorithms augmented with proposed regularization (ASD) outperform compared to their original form.

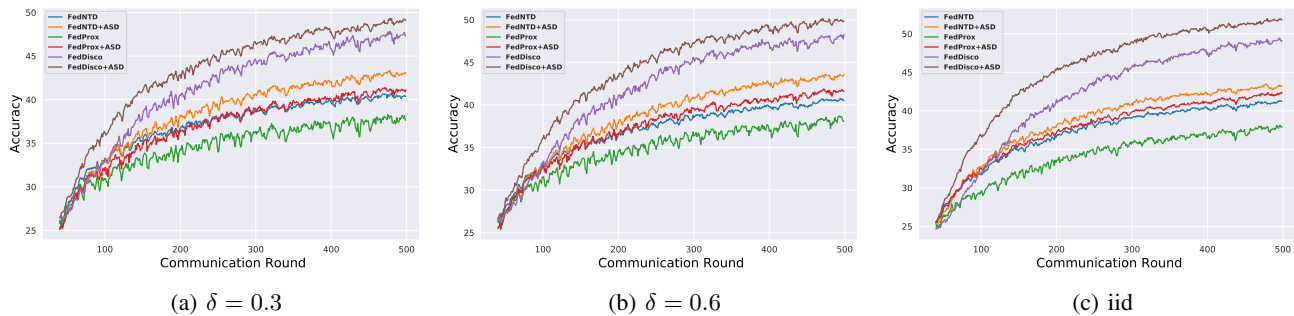


Figure 8. Test Accuracy vs Communication rounds: Comparison of algorithms with  $\delta = 0.3$ ,  $\delta = 0.6$  and iid data partitions on CIFAR-100 dataset. All the algorithms augmented with proposed regularization (ASD) outperform compared to their original form.

## G. Privacy of Proposed Method

In our method, which is ASD regularizer, the adaptive weights are computed by the client without depending on the server and it does not assume access to any auxiliary data at the server as assumed in methods such as FedCAD (He et al., 2022b) and FedDF (Lin et al., 2020). In our method, only model parameters are communicated with the server similar to FedAvg (McMahan et al., 2017). Thus our privacy is similar to the FedAvg method at the same time obtaining significant improvements in the performance.

## H. Hessian Analysis

In the Table 7 we analyze the top eigenvalue and the trace of the Hessian for all the algorithms. We observe that when ASD is used with the algorithms, it consistently improves the accuracy and reduces the top eigenvalue and the trace of the Hessian, this implies that ASD helps in converging to the flat minimum which is a typical indicator of better generalization. We consider the CIFAR-100 non-iid partition of  $\delta = 0.3$ .

Table 7. The table shows the impact of ASD on the algorithms on CIFAR-100 Dataset. We consistently see that the top eigenvalue and the trace of the Hessian decrease and the Accuracy improves when ASD is used. This suggests that using ASD makes the global model reach to a flat minimum for better generalization.

Algorithm	Top Eigenvalue ↓	Trace ↓	Accuracy ↑
FedAvg	53.6	8516	38.67
FedAvg + ASD	<b>12.3</b>	<b>2269</b>	<b>42.35</b>
FedProx	45.2	8683	37.79
FedProx + ASD	<b>11.9</b>	<b>2663</b>	<b>41.31</b>
FedDyn	49.4	6675	47.29
FedDyn + ASD	<b>14.2</b>	<b>2241</b>	<b>48.41</b>
FedNTD	<b>16.3</b>	3517	40.40
FedNTD + ASD	17.5	<b>2840</b>	<b>43.01</b>
FedSAM	19.04	4022	40.89
FedSAM + ASD	<b>6.0</b>	<b>1339</b>	<b>43.99</b>
FedDisco	46.7	8771	38.97
FedDisco + ASD	<b>12.2</b>	<b>2334</b>	<b>41.55</b>
FedSpeed	51.9	6937	47.39
FedSpeed + ASD	<b>14.6</b>	<b>2063</b>	<b>49.16</b>

---

## I. Proofs of Propositions:

We rewrite the adaptive weighting equations for convenience as below.

$$\alpha_k^i = \frac{\hat{\alpha}_k^i}{\sum_{i \in B} \hat{\alpha}_k^i} \quad (17)$$

and  $\hat{\alpha}_k^i$  is defined as below Eq. 18

$$\hat{\alpha}_k^i \triangleq \frac{\exp(-\mathcal{H}(x^i))}{p_k^{y^i}} \quad (18)$$

$$\alpha_i^k = \frac{\hat{\alpha}_i^k}{\sum_{i \in B} \hat{\alpha}_i^k} \quad (19)$$

**Proposition I.1.**  $\inf_{\mathbf{w} \in \mathbb{R}^d} G_d(\mathbf{w}, \lambda)$  is 1,  $\forall \lambda$

*Proof.*

$$G_d = \frac{\frac{1}{K} \sum_k \|\nabla f_k\|^2}{\|\nabla f\|^2} \quad (20)$$

$$\|\nabla f\|^2 = \left\| \frac{1}{K} \sum_k \nabla f_k \right\|^2 \quad (21)$$

Apply Jenson's inequality we get the desired result.

$$\|\nabla f\|^2 \leq \frac{1}{K} \sum_k \|\nabla f_k\|^2 \quad (22)$$

□

**Lemma I.2.** For any function of the form  $\zeta(x) = \frac{ax^2+bx+c_n}{ax^2+bx+c_d}$  satisfying  $c_n > c_d$ ,  $\exists x_c \geq 0$  such that  $\frac{d\zeta(x)}{dx} < 0 \forall x \geq x_c$

*Proof.*

$$\frac{d\zeta(x)}{dx} = \frac{(2ax+b)(ax^2+bx+c_d) - (2ax+b)(ax^2+bx+c_n)}{(ax^2+bx+c_d)^2} \quad (23)$$

By re-arranging and simplifying the above we get the following

$$\frac{d\zeta(x)}{dx} = \frac{2x(ac_d - ac_n) + b(c_d - c_n)}{(a_d x^2 + bx + c_d)^2} \quad (24)$$

We are interested in knowing when the numerator is negative.

$$x2a(c_d - c_n) \leq b(c_n - c_d) \quad (25)$$

Since  $c_n > c_d$ , we have

$$x2a(c_n - c_d) \geq -b(c_n - c_d) \implies x \geq \frac{-b}{2a} \quad (26)$$

assuming  $x_c = \left| \frac{-b}{2a} \right|$

We have the desired condition for  $x \geq x_c$

This concludes the proof. □

**Proposition I.3.** *When the class conditional distribution across the clients is identical, i.e.,  $\mathbb{P}_k(x | y) = \mathbb{P}(x | y)$  then  $\nabla f_k(\mathbf{w}) = \sum_c p_k^c (\mathbf{g}_c + \lambda \gamma_k^c \tilde{\mathbf{g}}_c)$ , where  $\mathbf{g}_c = \nabla \mathbb{E}[l(\mathbf{w}; x, y) | y = c]$ , and  $\tilde{\mathbf{g}}_c = \nabla \mathbb{E}[\exp(-\mathcal{H}(x)) \mathcal{D}_{KL}(q_g(x) || q_k(x)) | y = c]$  where  $\gamma_k^c = \frac{1}{p_k^c}$ .*

*Proof.* We re-write the equations for  $f_k(\mathbf{w})$  from Sec 3.3 of main paper,  $L_k(\mathbf{w})$  and  $L_k^{ASD}(\mathbf{w})$  from the Sec 3.2 of main paper for convenience.

$$f_k(\mathbf{w}) = L_k(\mathbf{w}) + \lambda L_k^{ASD}(\mathbf{w}) \quad (27)$$

$$L_k(\mathbf{w}) = \mathbb{E}_{x, y \in D_k} [l_k(\mathbf{w}; (x, y))] \quad (28)$$

$$L_k^{ASD}(\mathbf{w}) \triangleq \mathbb{E}[\alpha_k(x, y) \mathcal{D}_{KL}(q_g(x) || q_k(x))] \quad (29)$$

By applying the tower property of expectation, we expand Eq. 28 as below

$$L_k(\mathbf{w}) = \sum_c p_k^c \mathbb{E}[l_k(\mathbf{w}; x, y) | y = c] \quad (30)$$

If we assume the class-conditional distribution across the clients to be identical the value of  $\mathbb{E}[l_k(\mathbf{w}; x, y) | y = c]$  is same for all the clients. Under such assumptions, we can drop the client index  $k$  and rewrite the Eq. 30 as follows

$$L_k(\mathbf{w}) = \sum_c p_k^c \mathbb{E}[l(\mathbf{w}; x, y) | y = c] \quad (31)$$

$$\nabla L_k(\mathbf{w}) = \sum_c p_k^c \nabla \mathbb{E}[l(\mathbf{w}; x, y) | y = c] \quad (32)$$

We further simplify the notation by denoting  $\mathbf{g}_c = \nabla \mathbb{E}[l(\mathbf{w}; x, y) | y = c]$ .

$$\nabla L_k(\mathbf{w}) = \sum_c p_k^c \mathbf{g}_c \quad (33)$$

To make the analysis tractable, In Eq. 18, we use the un-normalized weighting scheme as the constant can be absorbed into  $\lambda$ . we can re-write Eq. 18 as below

$$\hat{\alpha}_k^i = \gamma_k^y \exp(\mathcal{H}(x)) \quad (34)$$

where  $\gamma_k^y = \frac{1}{p_k^y}$  With the above assumptions we can interpret the Eq. 29 as follows.

$$L_k^{ASD} = \mathbb{E}_{x, y \in D_k} [l_k^{dist}(\mathbf{w}; (x, y))] \quad (35)$$

where  $l_k^{dist}(\mathbf{w}; (x, y)) = \gamma_k^y \exp(-\mathcal{H}(x)) \mathcal{D}_{KL}(q_g(x) || q_k(x))$ .

By following the similar line of arguments from Eq. 30 to Eq. 32 we can write the following

$$\nabla L_k^{ASD}(\mathbf{w}) = \sum_c p_k^c \tilde{\mathbf{g}}_c \gamma_k^c \quad (36)$$



$$\nabla f_k(\mathbf{w}) = \sum_c p_k^c (\mathbf{g}_c + \lambda \gamma_k^c \tilde{\mathbf{g}}_c) \quad (37)$$

□

**Lemma I.4.** If  $c_n = \sum_{k=1}^K \sum_{c=1}^C (p_k^c)^2$ ,  $c_d = \sum_{k=1}^K \sum_{k2=1}^K \sum_{c=1}^C (p_{k1}^c p_{k2}^c)$ . where  $p_k^c \geq 0 \forall k, c$ , and  $\sum_{c=1}^C p_k^c = 1$ , then  $\frac{c_n}{c_d} \geq 1$ .

*Proof.* We need to show that

$$\frac{\sum_{k=1}^K \sum_{c=1}^C (p_k^c)^2}{\sum_{k1=1}^K \sum_{k2=1}^K \sum_{c=1}^C (p_{k1}^c p_{k2}^c)} \geq \frac{1}{K} \quad (38)$$

By rewriting the denominator we get

$$\frac{\sum_{k=1}^K \sum_{c=1}^C (p_k^c)^2}{\sum_{c=1}^C (\sum_{k=1}^K (p_k^c))^2} \geq \frac{1}{K} \quad (39)$$

Consider rewriting the denominator of the L.H.S of above equation.

$$\sum_{c=1}^C (\sum_{k=1}^K (p_k^c))^2 = \sum_{c=1}^C ((\mathbf{p}^c)^\top \mathbf{1})^2 \quad (40)$$

where  $\mathbf{p}^c = [p_1^c p_2^c \dots p_K^c]^\top$  and  $\mathbf{1}$  is the all one vector of size  $K$

Applying the Cauchy Schwartz inequality to the R.H.S of the Eq. 40 we get the following.

$$\sum_{c=1}^C ((\mathbf{p}^c)^\top \mathbf{1})^2 \leq \sum_{c=1}^C \sum_{k=1}^K (p_k^c)^2 K \quad (41)$$

By combining the Eq. 40 and Eq. 41 the result follows. □

**Proposition I.5.** When the class-conditional distribution across the clients is the same, and the Assumption 3.3 holds then  $\exists$  a range of values for  $\lambda$  such that whenever  $\lambda \geq \lambda_c$  we have  $\frac{dG_d}{d\lambda} < 0$  and  $G_d(\mathbf{w}, \lambda) < G_d(\mathbf{w}, 0)$ .

*Proof.*

$$G_d = \frac{\frac{1}{K} \sum_{k=1}^K \|\nabla f_k\|^2}{\|\nabla f\|^2} \quad (42)$$

From Sec 3.2 of the main paper we have the following, We drop the argument  $\mathbf{w}$  for the functions  $f_k$  to simplify the notation

$$\nabla f_k = \sum_{c=1}^C p_k^c (g_c + \lambda \gamma_k^c \tilde{g}_c) \quad (43)$$

$$\begin{aligned} \|\nabla f_k\|^2 &= \sum_{c1=1}^C \sum_{c2=1}^C p_k^{c1} p_k^{c2} (\mathbf{g}_{c1}^\top + \lambda \gamma_k^{c1} \tilde{\mathbf{g}}_{c1}^\top) (\mathbf{g}_{c2} + \lambda \gamma_k^{c2} \tilde{\mathbf{g}}_{c2}) \\ &= \sum_{c1=1}^C \sum_{c2=1}^C p_k^{c1} p_k^{c2} (\mathbf{g}_{c1}^\top \mathbf{g}_{c2} + \lambda \gamma_k^{c2} \mathbf{g}_{c1}^\top \tilde{\mathbf{g}}_{c2} + \lambda \gamma_k^{c1} \tilde{\mathbf{g}}_{c1}^\top \mathbf{g}_{c2} + \lambda^2 \gamma_k^{c2} \gamma_k^{c1} \tilde{\mathbf{g}}_{c1}^\top \tilde{\mathbf{g}}_{c2}) \\ &\approx \sum_{c=1}^C (p_k^c)^2 (\mathbf{g}_c^\top \mathbf{g}_c) + \lambda \sum_{c1=1}^C \sum_{c2=1}^C p_k^{c1} \mathbf{g}_{c1}^\top \tilde{\mathbf{g}}_{c2} + \lambda \sum_{c1=1}^C \sum_{c2=1}^C p_k^{c2} \tilde{\mathbf{g}}_{c1}^\top \mathbf{g}_{c2} + \lambda^2 \sum_{c=1}^C (p_k^c)^2 \gamma_k^c \gamma_k^c \tilde{\mathbf{g}}_c^\top \tilde{\mathbf{g}}_c \\ &= \sum_{c=1}^C (p_k^c)^2 + 2\lambda \sum_{c1=1}^C \sum_{c2=1}^C p_k^{c1} \mathbf{g}_{c1}^\top \tilde{\mathbf{g}}_{c2} + \lambda^2 C \end{aligned} \quad (44)$$

In the above equation the second equality is obtained by simply expanding the product, the third approximation by weakly correlated assumption of the gradients. The last two equalities used the fact that  $\gamma_k^c = \frac{1}{p_k^c}$ . We also assume that gradients are normalized to unit magnitude.

Finally, we have the following

$$\begin{aligned} \frac{1}{K} \sum_{k=1}^K \|\nabla f_k\|^2 &= \frac{1}{K} \left( \sum_{k=1}^K \sum_{c=1}^C (p_k^c)^2 + 2\lambda \sum_{k=1}^K \sum_{c_1=1}^C \sum_{c_2=1}^C p_k^{c_1} \mathbf{g}_{c_1}^\top \tilde{\mathbf{g}}_{c_2} + \lambda^2 K C \right) \\ &= \frac{1}{K^2} (a_n \lambda^2 + b_n \lambda + c_n) \end{aligned} \quad (45)$$

where

$$a_n := K^2 C \quad (46)$$

$$b_n := 2K \sum_{k=1}^K \sum_{c_1=1}^C \sum_{c_2=1}^C p_k^{c_1} \mathbf{g}_{c_1}^\top \tilde{\mathbf{g}}_{c_2}$$

$$c_n := K \sum_{k=1}^K \sum_{c=1}^C (p_k^c)^2 \quad (47)$$

$$\begin{aligned} \|\nabla f\|^2 &= \left\| \frac{1}{K} \sum_{k=1}^K \sum_{c=1}^C p_k^c (\mathbf{g}_c + \lambda \gamma_k^c \tilde{\mathbf{g}}_c) \right\|^2 \\ &= \frac{1}{K^2} \sum_{k_1=1}^K \sum_{k_2=1}^K \sum_{c_1=1}^C \sum_{c_2=1}^C p_{k_1}^{c_1} (\mathbf{g}_{c_1}^\top + \lambda \gamma_{k_1}^{c_1} \tilde{\mathbf{g}}_{c_1}^\top) p_{k_2}^{c_2} (\mathbf{g}_{c_2} + \lambda \gamma_{k_2}^{c_2} \tilde{\mathbf{g}}_{c_2}) \\ &\approx \frac{1}{K^2} \sum_{k_1=1}^K \sum_{k_2=1}^K \left( \sum_{c=1}^C p_{k_1}^c p_{k_2}^c (\mathbf{g}_c^\top \mathbf{g}_c) \right. \\ &\quad \left. + \sum_{c_1=1}^C \sum_{c_2=1}^C (\lambda p_{k_1}^{c_1} p_{k_2}^{c_2} \gamma_{k_2}^{c_2} \mathbf{g}_{c_1}^\top \tilde{\mathbf{g}}_{c_2} + \lambda p_{k_1}^{c_1} p_{k_2}^{c_2} \gamma_{k_2}^{c_2} \tilde{\mathbf{g}}_{c_1}^\top \mathbf{g}_{c_2} + \lambda^2 p_{k_1}^{c_1} p_{k_2}^{c_2} \gamma_{k_1}^{c_1} \gamma_{k_2}^{c_2} \tilde{\mathbf{g}}_{c_1}^\top \tilde{\mathbf{g}}_{c_2}) \right) \\ &= \frac{1}{K^2} \sum_{k_1=1}^K \sum_{k_2=1}^K \sum_{c=1}^C (p_{k_1}^c p_{k_2}^c) + \lambda \sum_{k_1=1}^K \sum_{k_2=1}^K \sum_{c_1=1}^C \sum_{c_2=1}^C p_{k_1}^{c_1} \mathbf{g}_{c_1}^\top \tilde{\mathbf{g}}_{c_2} + \lambda \sum_{k_1=1}^K \sum_{k_2=1}^K \sum_{c_1=1}^C \sum_{c_2=1}^C p_{k_2}^{c_2} \tilde{\mathbf{g}}_{c_1}^\top \mathbf{g}_{c_2} + \lambda^2 K^2 C \\ &= \frac{1}{K^2} \left( \sum_{k_1=1}^K \sum_{k_2=1}^K \sum_{c=1}^C (p_{k_1}^c p_{k_2}^c) + 2\lambda K \sum_{k=1}^K \sum_{c_1=1}^C \sum_{c_2=1}^C p_k^{c_1} \mathbf{g}_{c_1}^\top \tilde{\mathbf{g}}_{c_2} + \lambda^2 K^2 C \right) \\ &= \frac{1}{K^2} (a_d \lambda^2 + b \lambda + c_d) \end{aligned} \quad (48)$$

By defining

$$a_d := K^2 C \quad (49)$$

$$b_d := 2K \sum_{k=1}^K \sum_{c_1=1}^C \sum_{c_2=1}^C p_k^{c_1} \mathbf{g}_{c_1}^\top \tilde{\mathbf{g}}_{c_2}$$

$$c_d := \sum_{k_1=1}^K \sum_{k_2=1}^K \sum_{c=1}^C (p_{k_1}^c p_{k_2}^c) \quad (50)$$

By substituting Eq. 45 and Eq. 48 in Eq. 42 we get

$$G_d(\mathbf{w}, \lambda) = \frac{a_n \lambda^2 + b_n \lambda + c_n}{a_d \lambda^2 + b_d \lambda + c_d} \quad (51)$$

Comparing Eq. 46 and Eq. 49 we see that  $a := a_n = a_d$ ,  $b := b_n = b_d$ .

Also  $c_n > c_d$  assuming  $p_k^c$  is non-degenerate.

Using the Lemma I.2 on Eq. 51 we get the value of  $\lambda_b$  such that  $G_d(\mathbf{w}, \lambda)$  is reduced.

We also get  $\lambda \geq |\frac{-b}{a}|$  by analyzing the values of  $\lambda$  for which  $G_d(\mathbf{w}, \lambda) < G_d(\mathbf{w}, 0)$  holds.

Thus choosing the  $\lambda > \lambda_c = \sup_{b, -k^2 C \leq b \leq k^2 C} \max(\lambda_b, |\frac{-b}{a}|)$  guarantees  $G_d(\mathbf{w}, \lambda) < G_d(\mathbf{w}, 0)$ , for all  $\mathbf{w}$ .

This concludes the proof. □

## J. Discussion on Impact of Gradient Dissimilarity on the Convergence

We now study how the gradient diversity impacts the convergence of the FL algorithms such as FedProx and FedAvg. We omit the dependence of  $\lambda$  on  $B$ . (for these algorithms  $\lambda = 0$  so  $B$  is nothing but  $B(0)$  in our notation) We have the gradient dissimilarity assumption below

**Assumption J.1.**  $\frac{1}{K} \sum_k \|\nabla f_k(\mathbf{w})\|^2 \leq B^2 \|\nabla f(\mathbf{w})\|^2$

### J.1. FedProx

Suppose the functions  $f_k$  are lipschiltz smooth and their exists  $L_- > 0$  such that  $\mathbf{H}f_k \succeq L_- \mathbf{I}$ . With  $\bar{\mu} - L > 0$ , where  $\mu$  is FedProx regularization. If  $f_k$  satisfies the assumption J.1 then according to Theorem 6 of (Li et al., 2020) the FedProx, after  $T = \mathcal{O}(\frac{\Delta}{\rho \epsilon})$ . We have the gradient contraction as  $\frac{1}{T} \sum_{t=0}^{T-1} \mathbf{E} \|f(\mathbf{w}^t)\|^2 \leq \epsilon$ . The value of  $\rho$  is given below.

$$\rho = \frac{1}{\mu} - \frac{\gamma B}{\mu} - \frac{B(1+\gamma)\sqrt{(2)}}{\bar{\mu}\mu} - \frac{L(1+\gamma)^2 B^2}{2\bar{\mu}^2} - \frac{L(1+\gamma)^2 B^2}{K\bar{\mu}^2} (2\sqrt{2K} + 2) > 0 \quad (52)$$

for some  $\gamma > 0$  and  $\Delta = f(\mathbf{w}^0) - f(\mathbf{w}^*)$ ,  $f(\mathbf{w}^*)$  is the local minimum.

It can be seen that the convergence is inversely related to  $\rho$ . High value of  $\rho$  leads to faster convergence. From Eq. 52 we can see that  $\rho$  can be increased by decreasing the value of  $B$ . Thus reducing the value of  $B$  helps in better convergence.

### J.2. FedAvg

**Assumption J.2.** We now analyze the convergence of FedAvg, we consider the following assumptions  $\|\nabla f_k(\mathbf{x}) - \nabla f_k(\mathbf{y})\| = \beta \|\mathbf{x} - \mathbf{y}\|$  ( $\beta$  smoothness)

**Assumption J.3.** Gradients have bounded Variance.

Suppose that  $f(\mathbf{w})$  and  $f_k(\mathbf{w})$ , satisfies Assumptions J.1, J.2 and J.3. Let  $\mathbf{w}^* = \underset{\mathbf{w}}{\operatorname{arg\,min}} f(\mathbf{w})$  the local step-size be  $\alpha_l$ . The theorem V in (Karimireddy et al., 2020) shows that FedAvg algorithm will have contracting gradients. If Initial model is  $\mathbf{w}^0$ ,  $F = f(\mathbf{w}^0) - f(\mathbf{w}^*)$  and for constant  $M$ , then in  $R$  rounds, the model  $w^R$  satisfies  $\mathbb{E}[\|\nabla f(\mathbf{w}^R)\|^2] \leq \mathcal{O}(\frac{\beta M \sqrt{F}}{\sqrt{RLS}} + \frac{\beta B^2 F}{R})$ .

We see the convergence rate is  $\mathcal{O}(\frac{\beta M \sqrt{F}}{\sqrt{RLS}} + \frac{\beta B^2 F}{R})$ . We can see that convergence has a direct dependence on  $B^2$ . This is the only term that is linked to heterogeneity assumption. So the lower value of  $B$  implies faster convergence.

This motivates to have a tighter bound on heterogeneity. ASD achieves this by introducing the regularizer and choosing the appropriate value of  $\lambda$ . In the figure 9 we empirically we verify the impact of ASD on the convergence. We plot the smoothed estimates of the norm of the difference of the global model parameters between the successive communication rounds i.e  $\|\mathbf{w}^t - \mathbf{w}^{t-1}\|$ .

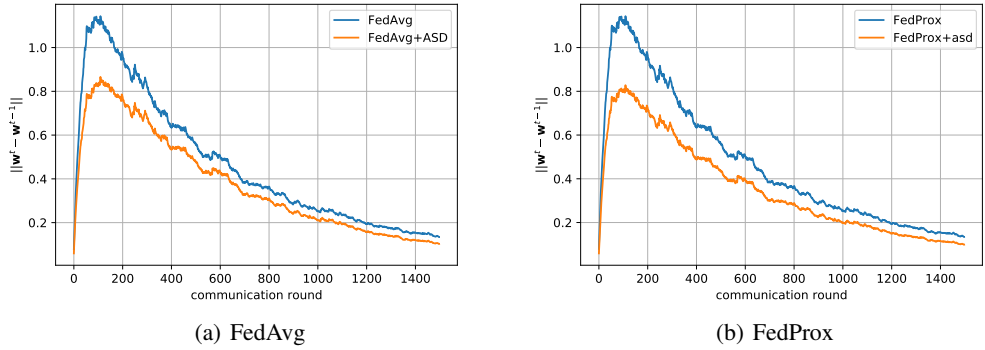


Figure 9. Impact of ASD on the convergence on CIFAR-100 dataset with non-iid partition of  $\delta = 0.3$